BIOMEDICAL ENGINEERING

10.1126/sciadv.1500887

Bioengineering a 3D integumentary organ system from iPS cells using an in vivo transplantation model

Ryoji Takagi,[1]* Junko Ishimaru,[1]* Ayaka Sugawara,[1]* Koh-ei Toyoshima,[2,3,4] Kentaro Ishida,[5] Miho Ogawa,[2,3,4] Kei Sakakibara,[1] Kyosuke Asakawa,[2] Akitoshi Kashiwakura,[1] Masamitsu Oshima,[5] Ryohei Minamide,[2] Akio Sato,[4] Toshihiro Yoshitake,[4] Akira Takeda,[4] Hiroshi Egusa,[6] Takashi Tsuji[2,3,5†]

The integumentary organ system is a complex system that plays important roles in waterproofing, cushioning, protecting deeper tissues, excreting waste, and thermoregulation. We developed a novel in vivo transplantation model designated as a clustering-dependent embryoid body transplantation method and generated a bioengineered three-dimensional (3D) integumentary organ system, including appendage organs such as hair follicles and sebaceous glands, from induced pluripotent stem cells. This bioengineered 3D integumentary organ system was fully functional following transplantation into nude mice and could be properly connected to surrounding host tissues, such as the epidermis, arrector pili muscles, and nerve fibers, without tumorigenesis. The bioengineered hair follicles in the 3D integumentary organ system also showed proper hair eruption and hair cycles, including the rearrangement of follicular stem cells and their niches. Potential applications of the 3D integumentary organ system include an in vitro assay system, an animal model alternative, and a bioengineered organ replacement therapy.

INTRODUCTION

Organogenesis is a complex process involving tissue self-organization, cell-cell interactions, regulation of signaling molecules, and cell movement (*1*–*3*). Almost all organs arise from organ germs, which are induced by reciprocal epithelial-mesenchymal interactions in each organ-forming field (*4*). Current regenerative therapy uses tissue stem cell transplantation to restore damaged tissues and organs in a wide variety of diseases (*5*–*7*). Next-generation regenerative therapy consists of organ replacement regenerative therapy, which aims to reproduce the reciprocal epithelial-mesenchymal interactions during embryogenesis. This organ regeneration therapy represents a fundamental approach to treating patients who experience organ dysfunction as a result of disease, injury, or aging (*8*). Our recent studies provided the proof of concept that fully functional regeneration of ectodermal organs, such as teeth, hair follicles, and salivary and lachrymal glands, could be achieved with the transplantation of bioengineered organ germs using the organ germ method (*9*–*13*). However, organ-inductive stem cells in a wide variety of organs, except hair follicles, exist only during embryonic organogenesis (*2*). Thus, we must develop techniques to reconstitute a wide variety of bioengineered organ germs using pluripotent stem cells, such as embryonic stem (ES) cells and induced pluripotent stem (iPS) cells (*2*, *14*).

Pluripotent stem cells, such as ES and iPS cells, can be induced to differentiate into specific somatic cell lineages using cytokines that mimic the patterning and positioning signals during embryogenesis (*15*). In the embryo, patterning signals indicating body axis and organ-forming fields are strictly controlled by signaling centers according to the embryonic body plan (*16*). These complex pattern formation signals in local areas of the body may lack centralized organizing signals, as observed in the generation of teratomas, which include disorganized neural tissues, cartilage, muscle, and bronchial epithelia (*17*). Although it is difficult to control the development of specific types of compartmentalized tissues, several groups recently reported neuroectodermal and endodermal organs generated via the regulation of complex patterning signals during embryogenesis and self-formation of pluripotent stem cells in three-dimensional (3D) stem cell culture (*2*, *3*, *18*–*22*). However, ectodermal organs, such as the skin, hair follicles, teeth, and exocrine organs, have not been generated with sufficient reproducibility from pluripotent stem cells in 3D stem cell culture or by transplantation (*3*).

The integumentary organ system (IOS) is a complex system that plays important roles in waterproofing, cushioning, protecting deeper tissues, excreting waste, and thermoregulation. The integumentary organs include the skin and its appendages (hair, sebaceous glands, sweat glands, feathers, and nails) (*23*). The integumentary organs arise from organ germs through reciprocal epithelial-mesenchymal interactions in the skin field (*4*). During embryogenesis, the skin field forms through a regulated process of pattern formation, and its appendage organs are then induced through epithelial-mesenchymal interactions according to a typical Turing model of activator and inhibitor signals (*23*). Regeneration of the 3D IOS could contribute to regenerative therapies for patients with burns, scars, and alopecia, and could be used as a novel assay system for nonanimal safety testing of cosmetics and quasi-drugs (*5*, *24*). However, it is difficult to generate the complex 3D IOS using in vitro stem cell culture or in vivo transplantation models and to recapitulate the physiological functions of the skin using a bioengineered 3D IOS.

Here, we generated a bioengineered 3D IOS from iPS cells, which includes appendage organs such as hair follicles and sebaceous glands, using a novel in vivo transplantation model designated as the

[1]Department of Biological Science and Technology, Graduate School of Industrial Science and Technology, Tokyo University of Science, Noda, Chiba 278-8510, Japan. [2]Laboratory for Organ Regeneration, RIKEN Center for Developmental Biology, Kobe, Hyogo 650-0047, Japan. [3]Organ Technologies Inc., Minato-ku, Tokyo 105-0001, Japan. [4]Department of Regenerative Medicine, Plastic and Reconstructive Surgery, Kitasato University of Medicine, Sagamihara, Kanagawa 252-0374, Japan. [5]Research Institute for Science and Technology, Tokyo University of Science, Noda, Chiba 278-8510, Japan. [6]Division of Molecular and Regenerative Prosthodontics, Tohoku University Graduate School of Dentistry, Sendai, Miyagi 980-8575, Japan.
*These authors contributed equally to this work.
†Corresponding author. E-mail: t-tsuji@cdb.riken.jp

clustering-dependent embryoid body (CDB) transplantation method. We first developed the conditions for the induction of various epithelial germ layers in in vivo explants of iPS cells. Wnt signaling controlled the frequency of the 3D IOS, calculated by the number of hair follicles in the explants. After orthotopic transplantation of the bioengineered IOS into nude mice, the bioengineered hair follicles showed full functionality, including the ability to undergo repeated hair cycles through the rearrangement of various stem cell niches. Our current study thus demonstrates the development of a functional bioengineered 3D IOS and the realization of organ replacement therapy using iPS cells.

RESULTS

In vivo induction of epithelial tissue using a CDB transplantation method

To generate various epithelia from iPS cells, we first developed a CDB transplantation method as an in vivo transplantation model. To form the complete three-germ-layer epithelial tissue from iPS cells, we established iPS cells from murine gingiva (Fig. 1A) (*25*). In an in vitro culture of iPS cells (3000 cells per well of a 96-well plate), iPS cells formed embryoid bodies (EBs) in 3 days, and the EBs were allowed to grow for 1 week (Fig. 1B). The relative mRNA expression levels of undifferentiated iPS markers (*Nanog*) were significantly reduced over the culture period (Fig. 1C and table S1). By contrast, neural crest markers, such as *Nestin* and *Pax3*, were significantly increased on day 7 in culture (Fig. 1C). In an immunohistochemical analysis of EBs after 7 days in culture, we observed that the iPS cell–derived EBs had differentiated into both epithelial and mesenchymal cells (Fig. 1D). EBs expressed Sox2 and p63 as integumentary markers and expressed Sox17 as an endodermal epithelial marker. EBs also expressed proteins for the neural progenitor marker Pax6 and for neural crest markers such as Snail and Twist (Fig. 1D). These results indicated that both epithelial and mesenchymal cells were generated in iPS cell–derived EBs after 7 days in culture.

We next transplanted these EBs under various conditions into the subrenal capsule of severe combined immunodeficient (SCID) mice in vivo. Both single iPS cells and single EB transplants formed teratoma-like tissues, which contained three germ layers, including neural tissue, muscle, cartilage, and bronchial epithelia, as reported previously (Fig. 1E, top and middle) (*26*). By contrast, in multiple EBs transplanted using collagen gel, which contained more than 30 EBs cultured for 7 days under nonadhesive conditions (Fig. 1F), cystic epithelia were observed in the CDB transplants (Fig. 1E, bottom). The tissue weight of CDB transplants was heavy compared with single EB transplants, and organ formation was observed in 4 to 9 g of explants (Fig. 1G). The ratio of cystic tissue area in CDB transplants was significantly larger than that in explants of single iPS cells and single EB transplants (Fig. 1H and fig. S1).

We next characterized the types of epithelium generated in the in vivo explants using the CDB transplantation method, such as ectodermal epithelium, nerve tissue, integument, and endodermal epithelium, including the respiratory tract and gastrointestinal tube, by histochemical analyses with specific antibodies for CK5, CK10, Muc2, Cdx2, Pax6, villin, Tuj1, CC10, and E-cadherin (Fig. 1I and fig. S2). In the explants, we identified various types of epithelium arising from the three germ layers, including ectodermal epithelium (CK5-positive), integument (CK10-positive), and endodermal epithelium, including the respiratory tract (Muc2-positive, CC10-positive, and CK10-negative) and gastrointestinal tube (villin-positive and Cdx2-positive). Although the transplantation of single ES or iPS cells induced epithelium at low efficiency (*27*), the incidence ratio of epithelium was statistically constant in explants generated via the CDB transplantation method (Fig. 1J). These results indicate that our CDB transplantation method reproduced various epithelia.

Bioengineered 3D IOS in iPS cell–derived explants generated using the CDB transplantation method

In the iPS cell–derived explants generated via the CDB transplantation method, we observed that Wnt10b, which regulates the dermal papilla (DP) (*28*–*30*) and the subcutaneous adipose tissue (*31*) derived from neural crest origin, induced the bioengineered hair follicles and developed the stage of hair follicles compared with the not-stimulated condition (Fig. 2A). The morphology of EBs and the expression of Sox2, p63, Sox17, Pax6, Snail, and Twist were not different with or without Wnt10b signaling (Fig. 1D and fig. S3). The hair shaft in the explant is black (Fig. 2A), although the hair shaft of the SCID mouse is white, indicating that hair follicles contain melanocytes that originate from iPS cell–derived neural crest cells. Although the frequencies in the explants with or without Wnt10b signaling were not different (Fig. 2B), the number of bioengineered hair follicles in the CDB explants treated with Wnt10b was drastically higher than that of the explants without Wnt10b (Fig. 2C). In the explants treated with Wnt10b, the bioengineered hair shaft, which was measured from the tip of the hair shaft to the DP, was longer than that in the explants without Wnt10b (Fig. 2D). Moreover, the hair follicles in explants treated with Wnt10b were abundant, and mature hair follicle structures included the dermal sheath, DP, sebaceous glands, and subcutaneous adipose tissue (Fig. 2E). The expression of *Shh*, *Msx2*, *Wnt10b*, β-*catenin*, and *Lef1* in the epithelium, and of *Bmp4* and *Notch1* in the mesenchyme of the bioengineered hair follicles in the CDB explants cultured with Wnt10b, was similar to that observed in natural skin on embryonic day 18.5 (fig. S4) (*11*). Thus, in the iPS cell–derived explants generated via the CDB transplantation method, we observed the bioengineered 3D IOS, including the skin, hair follicles, dermis, sebaceous glands, and subcutaneous adipose tissue. We confirmed these structures using other iPS cell clones, including a gingiva-derived iPS cell clone (ectodermal origin), the stomach-derived iPS-Stm-FB/gfp-99-1 clone (endodermal origin), and the hepatocyte-derived iPS-Hep-FB/Ng/gfp-103C-1 clone (endodermal origin) (*32*). The gingiva- and stomach-derived iPS cell clones, but not the iPS-Hep-FB/Ng/gfp-103C-1 clone, generated the bioengineered 3D IOS, including hair follicles. These results indicate that the generation of a bioengineered 3D IOS is not dependent on the origin of iPS cell clones from different germ layers because heterogeneity exists among iPS cell clones.

In hair follicles, various stem cell types are maintained in particular regions, such as CD34-, CK15-, and Sox9-positive follicle epithelial cells in the follicle stem cell niche of the bulge region (*33*, *34*), Lrig1-positive epithelial stem cells in the upper bulge outer root sheath region, and multipotent mesenchymal precursors in DP cells (*34*, *35*). The follicle variable region mediates the hair cycle, which depends on the activation of Lgr5-positive follicle epithelial stem cells during the telogen-to-anagen transition. In addition, the follicle epithelial stem cells in the bulge region connect to the calponin-positive arrector pili muscles (Fig. 2F). We next investigated whether various stem/progenitor cells and their niches were reconstructed in the EGFP-labeled bioengineered hair follicles of the CDB transplants, which were produced using the EGFP-labeled iPS cell clone. All cells composed of bioengineered 3D IOS showed green

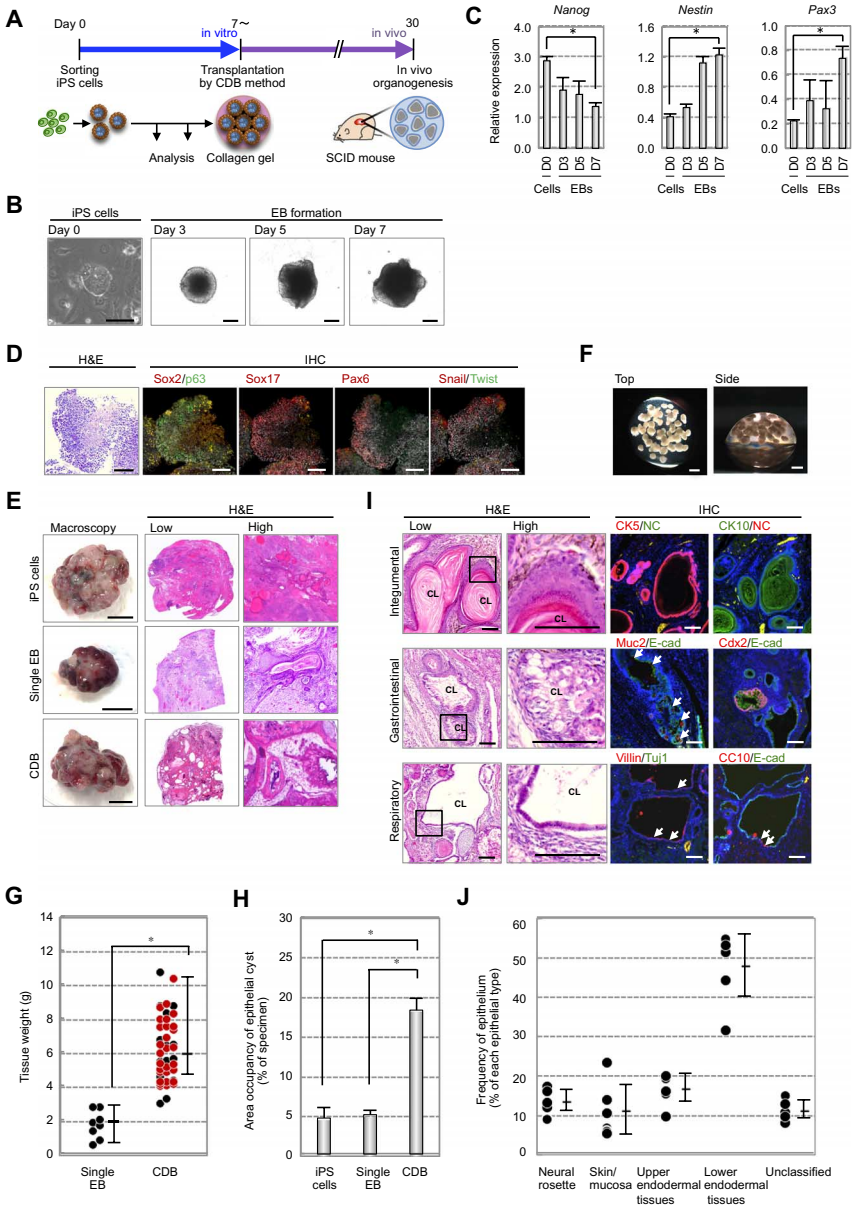

Fig. 1. Induction of epithelial tissues via the CDB transplantation method. (**A**) Schematic representation of EB cultures and the CDB transplantation method. (**B**) Phase-contrast images of iPS cells and the formation of EBs, which were cultured in nonadherent plastic wells for 3, 5, or 7 days. Scale bars, 100 μm. (**C**) mRNA expression levels of undifferentiated iPS cell markers (*Nanog*) and neural crest cell markers (*Nestin* and *Pax3*) during EB formation. *$P < 0.001$ by Student's *t* test. (**D**) Hematoxylin and eosin (H&E) staining and immunostaining of EBs, using antibodies of epithelial (Sox2/p63 and Sox17), neural progenitor (Pax6), and neural crest markers (Snail and Twist) after 7 days. The nuclei were stained using Hoechst 33258 (white). Scale bars, 50 μm. (**E**) Macroscopic photographs (left panels) and microscopy (H&E staining, center and right panels) of in vivo transplants under various transplantation conditions. The in vivo transplants of 3000 dissociated iPS cells (upper), single EBs (middle), and more than 30 EBs (lower) were placed in the subrenal capsule for 30 days and then analyzed. (**F**) Macroscopic photographs of multiple EB in a collagen gel before transplantation. Scale bars, 1 mm. (**G**) Weight of the in vivo transplants. The data are presented as the median ± maximum or minimum from individual experiments; $n = 8$ and $n = 48$ per experiment. Red circles indicate the cyst, including hair follicles, in the explants. *$P < 0.001$ by Student's *t* test. (**H**) The area occupancy of the cystic lumen in the whole specimens of in vivo transplants of the three types of conditions was compared. *$P < 0.001$ by Student's *t* test. (**I**) Histochemical and immunohistochemical analyses of the cystic epithelia in the in vivo explants of multiple iPS cell–derived EBs. Boxed areas in the left panels show H&E staining. To identify epithelial types, such as ectodermal epithelium, integument (top panels), and endodermal epithelium, including the gastrointestinal tube (middle panels) and respiratory tract (bottom panels), we analyzed CDB transplants by immunostaining with specific antibodies for CK5, CK10, Muc2, Cdx2, villin, CC10, Tuj1, and E-cadherin. The nuclei were stained using Hoechst 33258 (blue). To identify the nonspecific fluorescence signals in these immunohistochemical analyses, we performed the experiments under the conditions without specific antibodies against antigens [negative control (NC)]. Scale bars, 1 mm (low-magnification images) and 100 μm (high-magnification images). (**J**) The frequency of epithelial types in CDB transplants. Epithelial types in CDB transplants were classified based on the cell morphology and number count. The data are presented as the means ± SEM from individual experiments; $n = 5$.

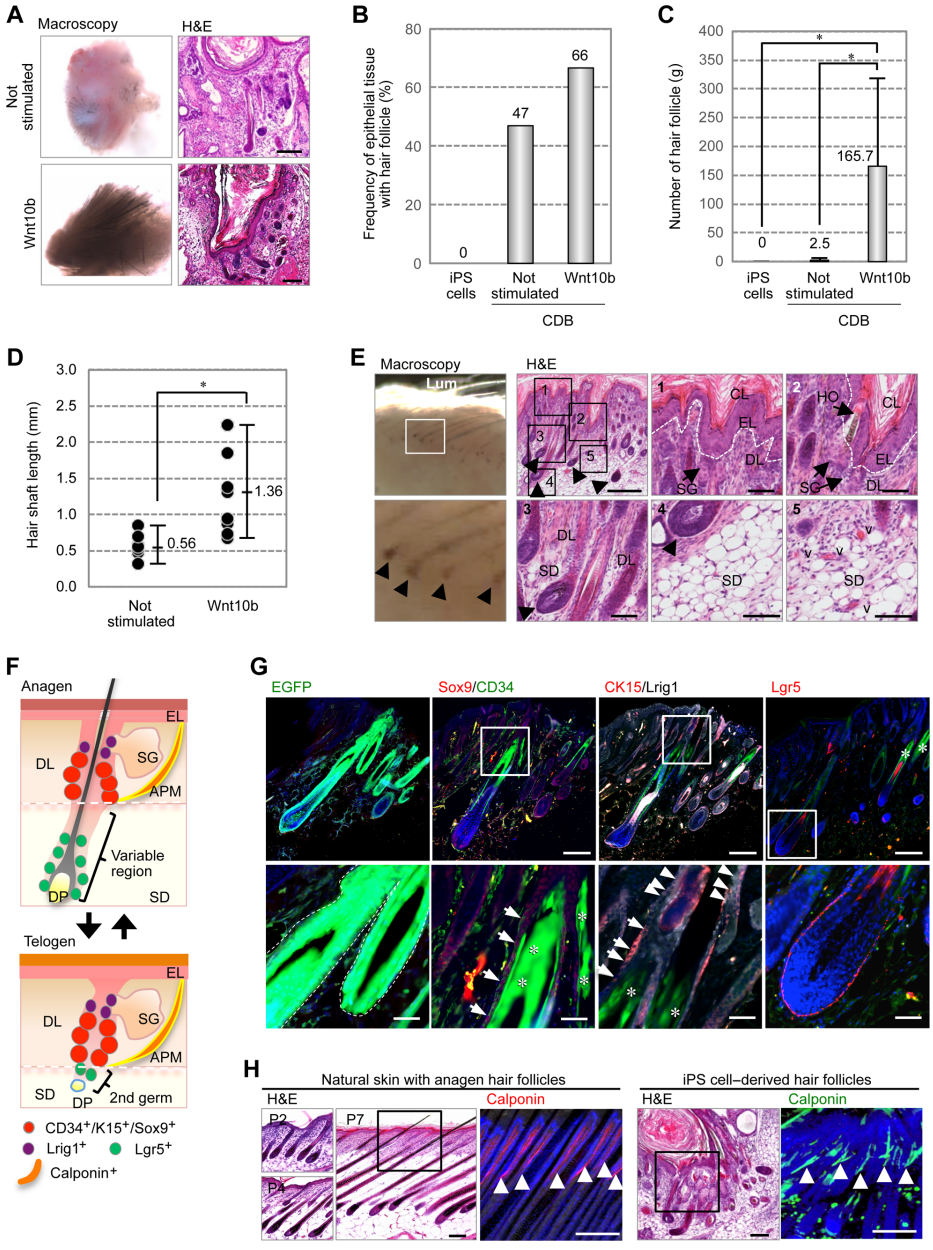

Fig. 2. Analysis of the bioengineered hair follicle induced from iPS cells via the CDB transplantation method. (**A**) Macroscopic (left panels) and microscopic (H&E staining; right panels) examination of the hair follicles and shafts in the CDB transplants. EBs were stimulated without Wnt10b (upper panels) or with Wnt10b (lower panel) on day 7. Scale bars, 100 μm. (**B**) Frequency of the epithelial tissue, including hair follicle, in CDB transplants. The data are presented as the means ± SEM from individual experiments; $n = 13$ (single iPS injection), $n = 49$ (CDB transplants without Wnt10b), and $n = 15$ (CDB transplants with Wnt10b). (**C**) Number of hair follicles in the CDB transplants. The data are presented as the means ± SEM from individual experiments; $n = 13$ (single iPS injection), $n = 74$ (CDB transplants without Wnt10b), and $n = 4$ (CDB transplants with Wnt10b). *$P < 0.001$ by Student's t test. (**D**) Comparative analysis of the length of hair shafts from the hair tip to the DP in CDB explants treated with or without Wnt10b. *$P < 0.05$ by Student's t test. (**E**) Histological analysis of the hair follicles and their surrounding tissues in iPS cell–derived bioengineered 3D IOSs. The isolated cystic structures with hair follicles were observed macroscopically (left panels). In the H&E analyses, the boxed areas in the low-magnification macroscopic views are shown at a higher magnification in other panels. CL, cystic lumen; EL, epidermal layer; DL, dermal layer; SD, subdermal tissue; SG, sebaceous gland; HO, hair opening; v, vessel. Scale bars, 500 μm (H&E; upper left) and 100 μm (others). (**F**) Schematic representation of stem/progenitor cells in the hair follicle and surrounding tissues on the skin at the anagen and telogen phases. APM, arrector pili muscle. (**G**) Immunohistochemical analyses of stem/progenitor cells in the follicles of natural pelage and enhanced green fluorescent protein (EGFP)–labeled iPS cell–derived bioengineered hair follicles. These samples were immunostained with anti-Sox9 (red), anti-CD34 (green), anti-CK15 (red), anti-Lrig1 (white), and anti-Lgr5 (red) antibodies. Arrows, epithelial cells of bulge regions; arrowheads, Lrig1-positive cells; *, background fluorescence of hair shafts. Scale bars, 200 μm (upper panels) and 50 μm (lower panels). (**H**) Histological and immunohistochemical analyses of the iPS cell–derived hair follicles and their surrounding tissues. Natural pelage and iPS cell–derived hair follicles were stained with calponin. Arrowheads indicate calponin-positive arrector pili muscles. Scale bars, 200 μm.

fluorescence (Fig. 2G, left panels). Sox9 and CD34 double-positive epithelial stem cells were also observed in the bulge region of the normal iPS-derived bioengineered hair follicles (Fig. 2G). Lrig1-positive epithelial stem cells and Lgr5-positive epithelial cells were also observed in the proper anatomical regions, which were detected in the upper and lower portions of the CK15-positive bulge region, respectively (Fig. 2G). The calponin-positive arrector pili muscle was connected to the bulge region epithelial cells of both the natural hair follicle and the bioengineered hair follicle (Fig. 2H). These results indicate that various follicle stem cells and the arrector pili muscles were correctly arranged in the bioengineered hair follicles constructed using the bioengineered 3D IOS, which was derived from iPS cells.

Orthotopic transplantation of the iPS cell–derived bioengineered 3D IOS

We next investigated whether the iPS cell–derived IOS could be transplanted into the cutaneous environment of adult nude mice (Fig. 3A, upper panel). We isolated male cystic tissues with hair follicles in the explants, cut them into small specimens containing 10 to 20 follicular units, and transplanted them onto the backs of female nude mice using a follicular unit transplantation method (Fig. 3A, lower panels). At 14 days and thereafter, we observed the eruption and growth of black hair shafts (n = 216; Fig. 3B). After 3 months, we did not observe tumorigenesis in the transplantation areas (n = 171). To confirm that the transplanted 3D IOS was of iPS cell origin, we performed Y-chromosome fluorescence in situ hybridization (Y-FISH) with male mouse–specific DNA probes (Fig. 3C and fig. S5). Y-FISH–positive cells were observed in the transplantation area (including the skin epithelium, dermis, sebaceous glands, intracutaneous adipose tissue, and hair follicles) of the cervical skin of recipient female mice. These results indicated that the bioengineered IOS could engraft in the cervical skin and revealed that it is of iPS cell origin. The engrafted hair follicle must establish proper connections with the surrounding tissues, such as the arrector pili muscles and nerve fibers. The hair follicles in the bioengineered 3D IOS had connected to calponin-positive arrector pili muscles in the correct polarization to iPS cell–derived follicles, which were identical to natural pelage follicles (Fig. 3D). Nerve fibers had also formed proper connections to the bulge region of the bioengineered hair follicles (Fig. 3D, lower panels). These results indicate that the iPS cell–derived hair follicles in the bioengineered IOS were correct in structure and established the proper connections to the surrounding tissues.

Analysis of iPS cell–derived hair species and distribution

We next investigated the hair species and their distribution in the bioengineered IOS in the cutaneous environment of recipient adult nude mice. The iPS cell–derived IOS produced all types of pelage hairs, including zigzag and awl/auchene and guard, in a similar population to the back skin of adult mice (Fig. 4, A and B) (*36*). We found that the distance between bioengineered hair follicles was not significantly different from that on the skin of normal mice (Fig. 4C). We further analyzed the distribution of hair shaft species in the transplanted iPS cell–derived IOS and compared the result with the natural skin of adult murine trunk region, including the body center and lumbar region of the side trunk lining on linea axillaris media (fig. S6). We also observed that the distribution of these hair species in the transplanted IOS was not significantly different from that in normal mice skin (fig. S6C). We further analyzed the hair cycles, which comprise alternating growth (hair growing) and regression (nongrowing) phases, of the iPS cell–derived hair follicles for 90 days (Fig. 4D). The iPS cell–derived follicles repeated the hair cycle at least three times during the transplantation period (Fig. 4D), and no significant differences in the hair cycle periods were found between natural and bioengineered follicles (both zigzag and awl/auchene and guard; Fig. 4E). These results suggest that the CDB transplantation method induced a skin field during early development by the subrenal capsule transplantation and generated the bioengineered IOS that behaved like natural mouse skin.

DISCUSSION

Our current findings reveal the generation of the bioengineered 3D IOS from iPS cells, including appendage organs such as hair follicles and sebaceous glands, with proper connections to surrounding tissues, including the epidermis, dermis, arrector pili muscles, fat, and nerve fibers, in an in vivo transplantation model—the CDB method. These findings significantly advance the technological development of bioengineered 3D IOS.

Studies of pluripotent stem cells have demonstrated the ability to generate whole embryos by tetraploid complementation in blastocysts and revealed that these cells can form teratomas, which include compartmentalized organized tissues derived from three germ layers, such as neural tissue (ectodermal), cartilage (mesenchymal), and gut/bronchial epithelia (endodermal), by an in vivo injection assay (*37*). Several cutaneous types of mature teratomas, such as cystic dermoids in the ovary and orbital regions, generate ectodermal organs, such as teeth and hair follicles (*17*). However, the molecular mechanisms underlying the development of these dermoids are still unknown. In an in vivo injection assay of ES and iPS cells, ectodermal organs could not be detected at a considerable frequency in pluripotent stem cell–derived teratomas. In 3D stem cell culture, bioengineered 3D tissues are limited to neuroectodermal and endodermal tissues (*2*). Thus, to generate a 3D IOS, we developed a novel CDB transplantation method to induce ectodermal tissues at a high frequency and successfully generated a 3D IOS in in vivo explants. In general, cultured EBs form an outer layer epithelial progenitor (*38*, *39*). Epithelium induction in our method may be due to the connection of the outer layer epithelium of each EB by self-assembly and self-formation in the explants. Furthermore, the frequency of hair follicles with sebaceous glands in the in vivo explants of our bioengineered 3D IOS could be controlled by Wnt signaling. Hence, our CDB transplantation method can be used to generate a bioengineered 3D IOS and contributes to our understanding of the molecular mechanisms of the onset of dermoid formation in vivo.

Wnt signaling pathways are essential for body patterning during embryogenesis and organ induction through epithelial-mesenchymal interactions (*40*). Wnt family molecules play important roles in forming an organ-forming field and the initial organ bud in both epithelial and mesenchymal tissues (*41*). Wnt10b signaling is known to play a key role in the progression of an initial organ bud to an organ germ, and also regulates the reciprocal epithelial-mesenchymal interactions of ectodermal organs, such as teeth, hair follicles, and exocrine organs (*28*). In hair follicle organogenesis, Wnt10b signaling regulates the differentiation from neural crest–derived mesenchyme into DP and the surrounding fat tissue (*30*, *42*, *43*). Here, the frequency of hair follicle formation, but not epithelial tissue formation, in in vivo explants was controlled by Wnt10b signaling in EBs. After treatment with Wnt10b on day 6 in culture, we detected the expression of neural crest

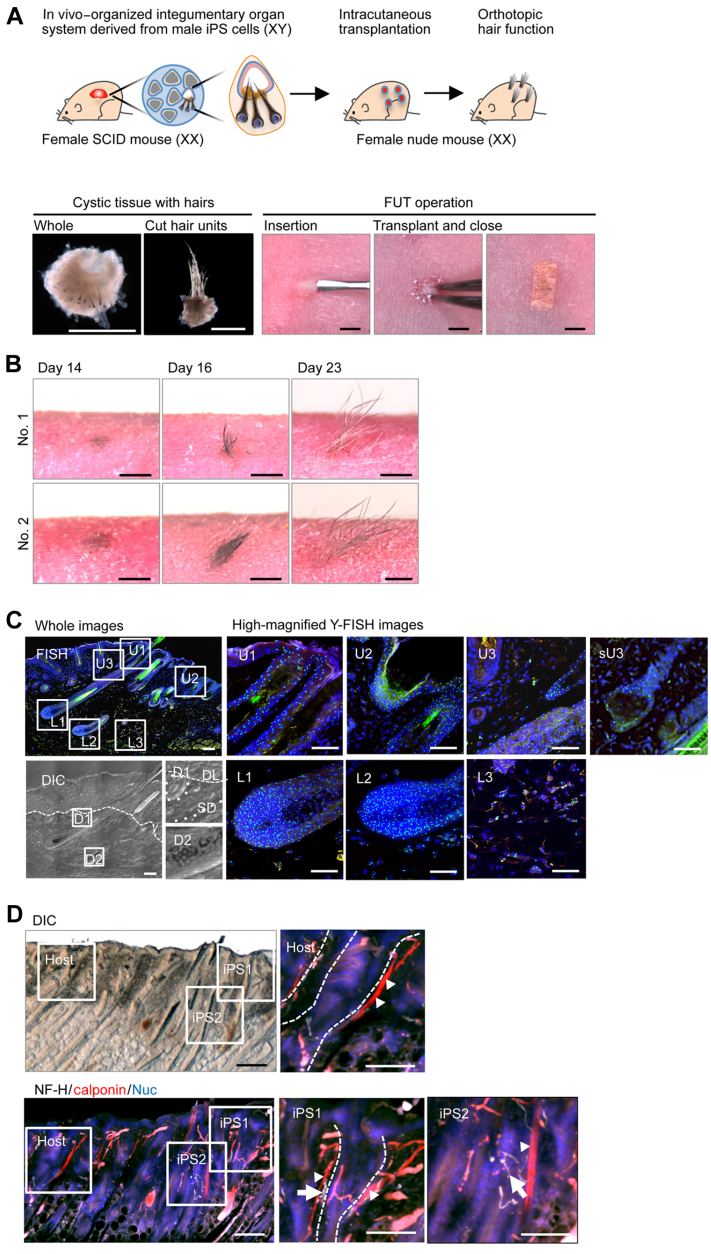

Fig. 3. Transplantation of the bioengineered 3D IOS. (**A**) Schematic representation of the methods used for the generation and transplantation of iPS cell–derived hair follicles. Cystic tissue with hair follicles was isolated and divided into small pieces containing 10 to 20 hair follicles (lower left panels). The small pieces were transplanted into the back skin of nude mice using a follicular unit transplantation (FUT) method developed in humans (lower right panels). Scale bars, 500 μm (lower left panels) and 1 mm (lower right panels). (**B**) Macromorphological observations of two independent engraftments into the dorsoventral skin of nude mice showing the eruption and growth of iPS cell–derived hair follicles. Scale bars, 1 mm. (**C**) Y-FISH analysis of the CDB transplants using male mouse–specific DNA probes. H&E and differential interference contrast (DIC) images are shown in the left panels. FISH images are shown in the upper left panel. Green and blue signals indicate Y-chromosome–positive cells and nuclei, respectively. Boxed areas in the FISH image are shown at a higher magnification in the right panels. Boxed areas U1 and U2 indicate the skin epithelium and upper region of the hair follicle. U3 indicates the bulge region. Boxed area sU3 indicates the Y-FISH–positive sebaceous gland isolated from fig. S5. Boxed areas L1 and L2 indicate the lower hair bulb region. Boxed area L3 indicates the intracutaneous adipose tissue. Broken lines in the differential interference contrast image indicate the outermost limit of the dermis. Scale bars, 200 μm (whole images) and 100 μm (high-magnification images). (**D**) Analysis of the integration with surrounding tissues, such as the arrector pili muscles and nerves, in the cervical skin of nude mice. The differential interference contrast images show black hair shafts derived from the bioengineered 3D IOS (origin: C57BL/6 mice) among the white hairs of nude mice. The arrector pili muscles and nerve fibers were analyzed by immunohistochemical staining using specific antibodies against calponin (red) for smooth muscle and neurofilament H (NF-H; white). The nuclei (Nuc) were stained using Hoechst 33258 (blue). The boxed areas in the left panels are shown at a higher magnification in the right panels. The arrows and arrowheads indicate nerve fibers and muscles connected with hair follicles, respectively. Broken lines indicate the outermost limit of each hair follicle. Scale bars, 200 μm (low-magnification photographs) and 100 μm (high-magnification photographs).

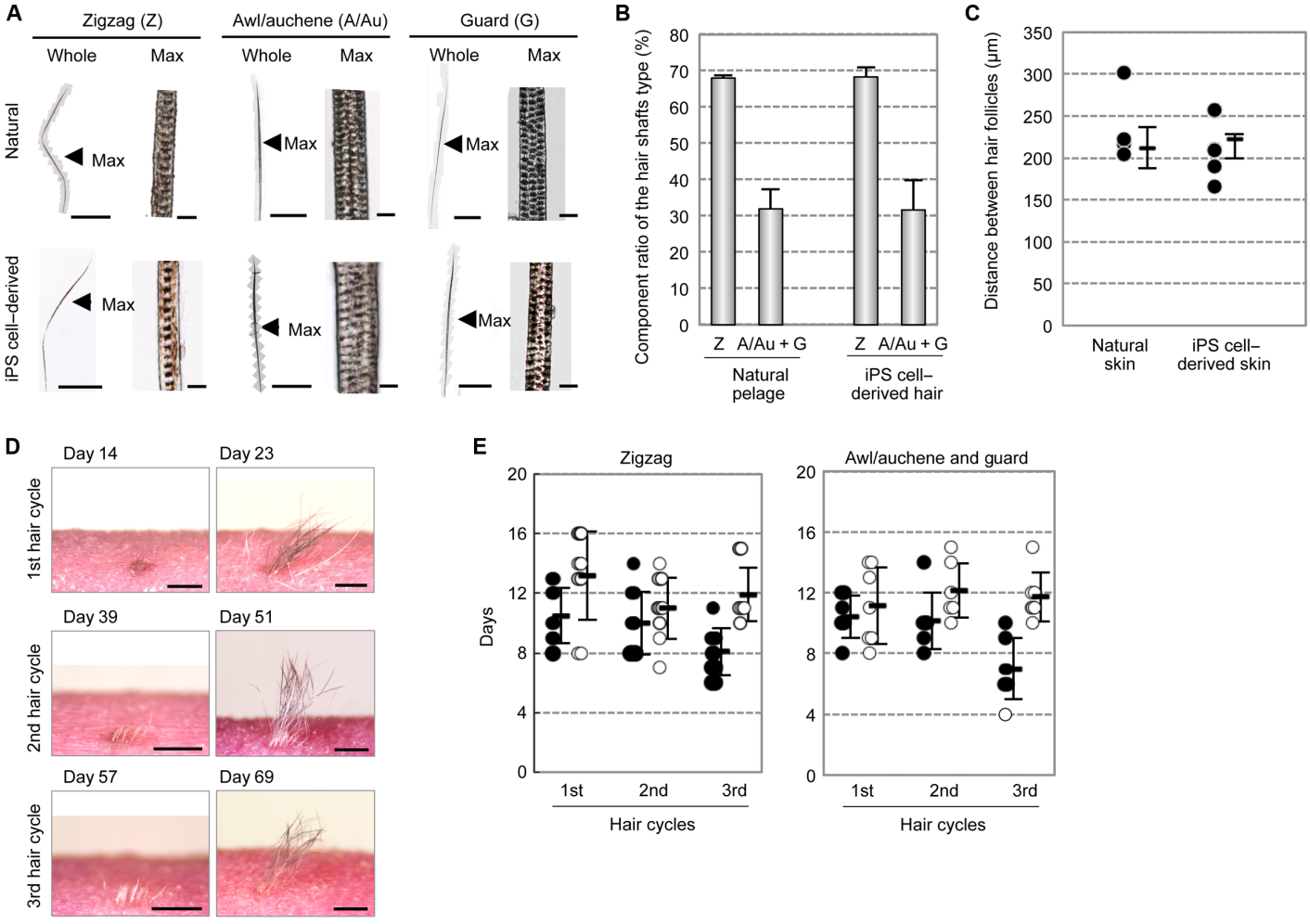

Fig. 4. Analysis of iPS cell–derived hair types and hair cycle. (**A**) Microscopic observation of the iPS cell–derived bioengineered hair shafts showing zigzag, awl/auchene, and guard hairs. The hair shafts were analyzed using light microscopy. Whole (left) and high-magnification (right) views are shown. Scale bars, 2 mm (low magnification) and 20 μm (high magnification). (**B**) Analysis of hair types, such as zigzag (Z), awl/auchene (A/Au), and guard (G), of natural mouse pelage and iPS cell–derived hair shafts. The hair types were determined by microscopic observations. The data are presented as the means ± SEM from six individual experiments; $n = 104$ (natural skin) and $n = 248$ (iPS cell–derived transplants). (**C**) Distance between hair shafts in natural pelage and iPS cell–derived bioengineered hair shafts. The distances were calculated by microscopic observations of H&E-stained sections. The data are presented as the means ± SEM from individual experiments; $n = 6$ (natural skin) and $n = 6$ (iPS cell–derived transplants). (**D**) Macromorphological observations at the anagen phase of the hair cycles in iPS cell–derived bioengineered hair. Scale bars, 1 mm. (**E**) Assessment of the hair growth (closed circles) and regression (open circles) phases of the bioengineered hair, including zigzag and awl/auchene and guard hair types. The data are presented as the means ± SEM; $n = 5$ (zigzag) and $n = 10$ (awl/auchene and guard).

markers, including *Nestin*, *Pax3*, *Snail*, and *Twist*. Therefore, our findings suggest that Wnt10b signaling plays important roles in the formation of hair follicles in the skin field, neural crest–derived melanocyte differentiation, and progression of organogenesis through reciprocal epithelial-mesenchymal interactions during morphogenesis.

For regenerative therapy in patients with burns, a cultured epithelial sheet is useful for the replacement of skin physiological functions, such as the protection of deeper tissues, waterproofing, and thermoregulation (*5*). However, it is well recognized that current therapies using cultured epithelial tissues suffer from critical issues, including aesthetics and the inability to excrete sweat and lipids from exocrine organs (*44*). In addition, artificial skin consisting of cultured epidermis and dermis without appendage organs and pores is often used for testing during the development of cosmetics and quasi-drugs, although this method has critical limitations related to the permeability of cosmetics and drugs and the reliability of physiological responses (*45*). By contrast, it is expected that bioengineered 3D IOS can overcome these issues (*46*). Here, we provide evidence for the generation of a 3D IOS from iPS cells using an in vivo transplantation model. The explants were fully functional and included hair follicles and sebaceous glands with proper connections to the surrounding tissues, such as the epithelium, dermis, fat, arrector pili muscles, and nerve fibers. Although the origin of nerve fibers is still unclear, nerve fibers would be innervated from host tissues. Our previous studies of ectodermal organ transplantations demonstrated that the innervation into the explants had been indicated from host tissues (*10*–*13*).

In conclusion, we generated a fully functional 3D IOS by the self-assembly of epithelial and mesenchymal stem cells from iPS cells using the CDB transplantation method. Our study contributes to the development of bioengineering technologies that will enable future regenerative therapies for patients with burns, scars, and alopecia. Further optimization of our technique using in vitro stem cell culture and humanization will contribute to the development of bioengineered IOS therapy as a prominent class of organ system replacement regenerative therapy and as a novel nonanimal assay system for cosmetics and quasi-drugs in the future.

METHODS

Cell culture of mouse iPS cells

The mouse iPS cell line "gingiva-derived iPS" was established by Egusa *et al.* (*25*) at Tohoku University. The iPS-Stm-FB/gfp-99-1 and iPS-Hep-FB/Ng/gfp-103C-1 lines were purchased from the RIKEN BioResource Center. All iPS cell lines were maintained in the presence of a mitomycin C–treated SNLP feeder layer on gelatin-coated dishes. The culture medium for these mouse iPS cells consisted of Dulbecco's modified Eagle's medium (DMEM) (Nacalai Tesque) supplemented with 15% fetal bovine serum (Biosera), 2 mM L-glutamine (Invitrogen), 1×10^{-4} M nonessential amino acids (Invitrogen), 1×10^{-4} M 2-mercaptoethanol (Invitrogen), penicillin (50 U/ml), and streptomycin (50 μg/ml; Invitrogen) (*25*).

Induction of mouse iPS cell differentiation

Mouse iPS cells were harvested by dissociation using 0.25% trypsin-EDTA (Invitrogen) with feeder cells. Then, dissociated cells were separated into iPS cells and feeder cells using Feeder Removal MicroBeads (MACS; Miltenyi Biotec). For EB culture, the iPS cells were reaggregated using Nunclon Sphera round-bottom 96-well plates (Thermo Fisher Scientific Inc.) in a culture medium (3000 cells/100 μl per well). Fresh medium was added to the culture on day 3, and Wnt10b (500 ng/ml; R&D Systems) was added on day 6.

Gene expression analysis by real-time PCR

Total RNA was isolated from mouse iPS cells or EBs using TRIzol reagent (Life Technologies) according to the manufacturer's protocol. Reverse transcription was performed with the PrimeScript II 1st strand cDNA Synthesis Kit (TaKaRa Bio). The mRNA expression levels were determined using SYBR Premix Ex Taq II (TaKaRa Bio), and the products were analyzed with an Applied Biosystems QuantStudio 12K Flex (Life Technologies). The data were normalized to β-actin expression. The primer pairs used for real-time polymerase chain reaction (PCR) are listed in table S1. For quantitative analysis, 32 to 48 EBs were analyzed in triplicate in each experiment, which was repeated at least three times.

Animals

C.B-17/lcr-*scid/scid*Jcl mice were purchased from CLEA Japan Inc., and C57BL/6NCrSlc and Balb/c nu/nu mice were purchased from Japan SLC Inc. Animal care and handling conformed to the National Institutes of Health guidelines, the requirements of the Tokyo University of Science Animal Care and Use Committee (permit no. N13008), and the Guidelines for Use of Laboratory Animals of RIKEN and Use Committee (AH26-02-3).

iPS cell–derived EB transplantation and extraction

EBs cultured for 7 days were selected, and 48 (not stimulated) and 32 (Wnt10b stimulated) EBs were sterilely placed in a 20-μl collagen gel drop (Nitta Gelatin Inc.). The collagen gel drop was transplanted into the subrenal capsules of 6-week-old C.B-17/lcr-*scid/scid*Jcl mice. Thirty days after the transplantation of iPS-EBs, the in vivo transplants were extracted, divided into five equal parts, and placed into DMEM (WAKO) containing 10% fetal calf serum (GIBCO), penicillin (100 U/ml; Sigma), streptomycin (100 mg/ml; Sigma), and 20 mM Hepes (Invitrogen) on ice. They were treated with collagenase (100 U/ml; Worthington) for 10 min at 37°C and washed with medium to separate the organs for in vivo transplants. The iPS cell–derived 3D IOS was dissected using a surgical knife under a microscope.

Engraftment of the iPS cell–derived 3D IOS

For hair follicle regeneration, the iPS cell–derived hair follicles, which were divided into small pieces containing 10 to 20 hair follicles, were intracutaneously transplanted into the back skin of 6-week-old Balb/c nu/nu mice, as previously described (*47*). Shallow stab wounds were made on the back skin of nude mice using a 20-gauge Ophthalmic V-Lance (Alcon Japan). The iPS cell–derived 3D IOSs were held so that the hair protruded from the skin surface. The transplantation sites were then covered with surgical bandage tape (Nichiban). To examine the engraftment of the transplants and to study the hair cycles of the bioengineered hairs, we observed all transplanted sites using the SteREO Lumar.V12 and AxioCam fluorescent stereoscopic microscope system (Carl Zeiss). Observations were made every 2 to 3 days.

Immunohistochemistry

Paraffin sections (10 μm) were stained with H&E and observed using an Axio Imager A1 (Carl Zeiss) or an Axio Scan.Z1 (Carl Zeiss). For fluorescent immunohistochemistry, frozen sections (10 and 100 μm) and paraffin sections (10 μm) were prepared and immunostained as previously described (*11*, *12*). Before immunostaining, frozen sections of EGFP-labeled samples were treated with or without Superfix (KURABO) for 30 min at room temperature. The primary antibodies used were as follows: CK5 (1:100, rabbit; Covance), CK10 (DE-K10) (1:100, rabbit; Abcam), Muc2 (H-300) (1:100, rabbit; Santa Cruz Biotechnology), Cdx2 (EPR2764Y) (1:250, rabbit; Abcam), Pax6 (1:200, rabbit; Covance), calponin (EP798Y) (1:250, rabbit; Abcam), CK15 (1:2000, chicken; Abcam), Sox9 (1:100, mouse; Abcam), CD34 (MEC 14.7) (1:100, rat; Abcam), Lrig1 (1:400, goat; R&D Systems), Lgr5 (1:100, rabbit; Abcam), neurofilament H (TA51) (1:500, rat; Chemicon), villin (C-19) (1:200, goat; Santa Cruz Biotechnology), CC10 (T-18) (1:100, goat; Santa Cruz Biotechnology), Tuj1 (TU-20) (1:200, mouse; Chemicon), and E-cadherin (36/E-Cadherin) (1:200, mouse; BD Biosciences) in blocking solution. The primary antibodies were detected using highly cross-absorbed Alexa Fluor 488 donkey anti-mouse immunoglobulin G (IgG; H + L) (1:500; Life Technologies), Alexa Fluor 488 goat anti-rat IgG (H + L) (1:500; Life Technologies), Alexa Fluor 488 donkey anti-rabbit IgG (H + L) (1:500; Life Technologies), Alexa Fluor 594 donkey anti-mouse IgG (H + L) (1:500; Life Technologies), Alexa Fluor 594 donkey anti-goat IgG (H + L) (1:500; Invitrogen), Alexa Fluor 594 donkey anti-rabbit IgG (1:500; Invitrogen), Alexa Fluor 594 goat anti-rabbit IgG (H + L) (1:500; Life Technologies), or Alexa Fluor 633 goat anti-rat IgG (H + L) (1:500; Invitrogen) with Hoechst 33258 dye (1:500; Dojindo) for 1 hour at room temperature. All fluorescence microscopy images were obtained with an LSM 780 confocal microscope (Carl Zeiss) or an Axio Scan.Z1 (Carl Zeiss).

Mouse Y-FISH

To detect male-origin iPS cell–derived 3D IOSs engrafted into female mouse skin, we performed mouse Y-FISH on 10-μm paraffin sections using fluorescein isothiocyanate–conjugated murine Y-chromosome probes (Chromosome Science Labo Inc.). All fluorescence microscopy images were captured on an LSM 780 confocal microscope (Carl Zeiss).

In situ hybridization

In situ hybridizations were performed using 10-μm frozen sections as described previously (*11*). Briefly, digoxigenin-labeled probes for specific transcripts were prepared by PCR with published primers. The mRNA expression patterns were visualized according to the immunoreactivity with anti-digoxigenin alkaline phosphatase–conjugated Fab fragments (Roche) according to the manufacturer's instructions.

Analyses of the distance between hair follicles and the distribution of hair shaft species

Skin samples from C57BL/6NCrSlc mice were dissected from three different regions, including the thorax, body center, and lumbar region of the side trunk lining on murine linea axillaris media. The iPS cell–derived IOSs, which were divided into small pieces containing 10 to 20 hair follicles from in vivo explants, were intracutaneously transplanted into the back skin of 6-week-old Balb/c nu/nu mice, as described above. The iPS cell–derived skins after transplantation were dissected at the first or second anagen phase. The natural skins and iPS cell–derived skin were fixed and placed horizontally on a plastic dish before macroscopic photographs were taken. To examine the hair types and distribution of the species of hair shafts, we observed all samples using the SteREO Lumar.V12 and AxioCam microscope system (Carl Zeiss). The distance between hair pores was measured with AxioVision Vs40 Image processing software (Carl Zeiss). The position of natural and iPS cell–derived hair pores, hair growth direction, and species of hair shafts (classified as zigzag and awl/auchene and guard) in 1-mm^2 portions were analyzed by the methods described previously (*36*).

SUPPLEMENTARY MATERIALS

Supplementary material for this article is available at http://advances.sciencemag.org/cgi/content/full/2/4/e1500887/DC1

Fig. S1. Analysis of the area of the cystic lumen.

Fig. S2. Histochemical and immunohistochemical analyses of the cystic epithelia in the in vivo explants of multiple iPS cell–derived EBs.

Fig. S3. Culture of iPS cells for EB formation.

Fig. S4. Gene expression in iPS cell–derived bioengineered hair follicle germs in a 3D IOS generated via the CDB transplantation method.

Fig. S5. Y-FISH analysis of the distribution of iPS cell–derived cells among the 3D IOSs grafted to the natural murine skin.

Fig. S6. Distribution of hair species of iPS cell–derived hairs.

Table S1. Primer sequences used in real-time PCR.

REFERENCES AND NOTES

1. M. Takeichi, Self-organization of animal tissues: Cadherin-mediated processes. *Dev. Cell* **21**, 24–26 (2011).
2. Y. Sasai, Next-generation regenerative medicine: Organogenesis from stem cells in 3D culture. *Cell Stem Cell* **12**, 520–530 (2013).
3. Y. Sasai, Cytosystems dynamics in self-organization of tissue architecture. *Nature* **493**, 318–326 (2013).
4. J. Pispa, I. Thesleff, Mechanisms of ectodermal organogenesis. *Dev. Biol.* **262**, 195–205 (2003).
5. B. K. Sun, Z. Siprashvili, P. A. Khavari, Advances in skin grafting and treatment of cutaneous wounds. *Science* **346**, 941–945 (2014).
6. T.-T. Sun, H. Green, Differentiation of the epidermal keratinocyte in cell culture: Formation of the cornified envelope. *Cell* **9**, 511–521 (1976).
7. A. Atala, Human stem cell-derived retinal cells for macular diseases. *Lancet* **385**, 487–488 (2015).
8. P. T. Sharpe, C. S. Young, Test-tube teeth. *Sci. Am.* **293**, 34–41 (2005).
9. K. Nakao, R. Morita, Y. Saji, K. Ishida, Y. Tomita, M. Ogawa, M. Saitoh, Y. Tomooka, T. Tsuji, The development of a bioengineered organ germ method. *Nat. Methods* **4**, 227–230 (2007).
10. E. Ikeda, R. Morita, K. Nakao, K. Ishida, T. Nakamura, T. Takano-Yamamoto, M. Ogawa, M. Mizuno, S. Kasugai, T. Tsuji, Fully functional bioengineered tooth replacement as an organ replacement therapy. *Proc. Natl. Acad. Sci. U.S.A.* **106**, 13475–13480 (2009).
11. K.-e. Toyoshima, K. Asakawa, N. Ishibashi, H. Toki, M. Ogawa, T. Hasegawa, T. Irié, T. Tachikawa, A. Sato, A. Takeda, T. Tsuji, Fully functional hair follicle regeneration through the rearrangement of stem cells and their niches. *Nat. Commun.* **3**, 784 (2012).
12. M. Ogawa, M. Oshima, A. Imamura, Y. Sekine, K. Ishida, K. Yamashita, K. Nakajima, M. Hirayama, T. Tachikawa, T. Tsuji, Functional salivary gland regeneration by transplantation of a bioengineered organ germ. *Nat. Commun.* **4**, 2498 (2013).
13. M. Hirayama, M. Ogawa, M. Oshima, Y. Sekine, K. Ishida, K. Yamashita, E. Ikeda, S. Shimmura, T. Kawakita, K. Tsubota, T. Tsuji, Functional lacrimal gland regeneration by transplantation of a bioengineered organ germ. *Nat. Commun.* **4**, 2497 (2013).
14. S. M. Wu, K. Hochedlinger, Harnessing the potential of induced pluripotent stem cells for regenerative medicine. *Nat. Cell Biol.* **13**, 497–505 (2011).
15. D. E. Cohen, D. Melton, Turning straw into gold: Directing cell fate for regenerative medicine. *Nat. Rev. Genet.* **12**, 243–252 (2011).
16. E. Walck-Shannon, J. Hardin, Cell intercalation from top to bottom. *Nat. Rev. Mol. Cell Biol.* **15**, 34–48 (2014).
17. F. A. Tavassoll, P. Devilee, Eds., *Pathology and Genetics of Tumours of the Breast and Female Genital Organs. World Health Organization Classification of Tumours* (IARC Press, Lyon, France, 2003), 432 pp.
18. M. Eiraku, N. Takata, H. Ishibashi, M. Kawada, E. Sakakura, S. Okuda, K. Sekiguchi, T. Adachi, Y. Sasai, Self-organizing optic-cup morphogenesis in three-dimensional culture. *Nature* **472**, 51–56 (2011).
19. H. Suga, T. Kadoshima, M. Minaguchi, M. Ohgushi, M. Soen, T. Nakano, N. Takata, T. Wataya, K. Muguruma, H. Miyoshi, S. Yonemura, Y. Oiso, Y. Sasai, Self-formation of functional adenohypophysis in three-dimensional culture. *Nature* **480**, 57–62 (2011).
20. T. Nakano, S. Ando, N. Takata, M. Kawada, K. Muguruma, K. Sekiguchi, K. Saito, S. Yonemura, M. Eiraku, Y. Sasai, Self-formation of optic cups and storable stratified neural retina from human ESCs. *Cell Stem Cell* **10**, 771–785 (2012).
21. K. R. Koehler, A. M. Mikosz, A. I. Molosh, D. Patel, E. Hashino, Generation of inner ear sensory epithelia from pluripotent stem cells in 3D culture. *Nature* **500**, 217–221 (2013).
22. C. L. Watson, M. M. Mahe, J. Múnera, J. C. Howell, N. Sundaram, H. M. Poling, J. I. Schweitzer, J. E. Vallance, C. N. Mayhew, Y. Sun, G. Grabowski, S. R. Finkbeiner, J. R. Spence, N. F. Shroyer, J. M. Wells, M. A. Helmrath, An in vivo model of human small intestine using pluripotent stem cells. *Nat. Med.* **20**, 1310–1314 (2014).
23. T.-X. Jiang, R. B. Widelitz, W.-M. Shen, P. Will, D.-Y. Wu, C.-M. Lin, H.-S. Jung, C.-M. Chuong, Integument pattern formation involves genetic and epigenetic controls: Feather arrays simulated by digital hormone models, *Int. J. Dev. Biol.* **48**, 117–135 (2004).
24. Y. Fukano, N. G. Knowles, M. L. Usui, R. A. Underwood, K. D. Hauch, A. J. Marshall, B. D. Ratner, C. Giachelli, W. G. Carter, P. Fleckman, J. E. Olerud, Characterization of an in vitro model for evaluating the interface between skin and percutaneous biomaterials. *Wound Repair Regen.* **14**, 484–491 (2006).
25. H. Egusa, K. Okita, H. Kayashima, G. Yu, S. Fukuyasu, M. Saeki, T. Matsumoto, S. Yamanaka, H. Yatani, Gingival fibroblasts as a promising source of induced pluripotent stem cells. *PLOS One* **5**, e12743 (2010).
26. K. Okita, M. Nakagawa, H. Hyenjong, T. Ichisaka, S. Yamanaka, Generation of mouse induced pluripotent stem cells without viral vectors. *Science* **322**, 949–953 (2008).
27. J. T. Fujii, G. R. Martin, Developmental potential of teratocarcinoma stem cells in utero following aggregation with cleavage-stage mouse embryos. *J. Embryol. Exp. Morphol.* **74**, 79–96 (1983).
28. S. Reddy, T. Andl, A. Bagasra, M. M. Lu, D. J. Epstein, E. E. Morrisey, S. E. Millar, Characterization of *Wnt* gene expression in developing and postnatal hair follicles and identification of *Wnt5a* as a target of Sonic hedgehog in hair follicle morphogenesis. *Mech. Dev.* **107**, 69–82 (2001).
29. J. Fu, W. Hsu, Epidermal Wnt controls hair follicle induction by orchestrating dynamic signaling crosstalk between the epidermis and dermis. *J. Invest. Dermatol.* **133**, 890–898 (2013).
30. Y. Ouji, F. Nakamura-Uchiyama, M. Yoshikawa, Canonical Wnts, specifically Wnt-10b, show ability to maintain dermal papilla cells. *Biochem. Biophys. Res. Commun.* **438**, 493–499 (2013).

31. S. E. Ross, N. Hemati, K. A. Longo, C. N. Bennett, P. C. Lucas, R. L. Erickson, O. A. MacDougald, Inhibition of adipogenesis by Wnt signaling. *Science* **289**, 950–953 (2000).
32. T. Aoi, K. Yae, M. Nakagawa, T. Ichisaka, K. Okita, K. Takahashi, T. Chiba, S. Yamanaka, Generation of pluripotent stem cells from adult mouse liver and stomach cells. *Science* **321**, 699–702 (2008).
33. R. J. Morris, Y. Liu, L. Marles, Z. Yang, C. Trempus, S. Li, J. S. Lin, J. A. Sawicki, G. Cotsarelis, Capturing and profiling adult hair follicle stem cells. *Nat. Biotechnol.* **22**, 411–417 (2004).
34. F. M. Watt, Mammalian skin cell biology: At the interface between laboratory and clinic. *Science* **346**, 937–940 (2014).
35. C. A. B. Jahoda, C. J. Whitehouse, A. J. Reynolds, N. Hole, Hair follicle dermal cells differentiate into adipogenic and osteogenic lineages. *Exp. Dermatol.* **12**, 849–859 (2003).
36. R. R. Driskell, A. Giangreco, K. B. Jensen, K. W. Mulder, F. M. Watt, Sox2-positive dermal papilla cells specify hair follicle type in mammalian epidermis. *Development* **136**, 2815–2823 (2009).
37. K. Takahashi, S. Yamanaka, Induction of pluripotent stem cells from mouse embryonic and adult fibroblast cultures by defined factors. *Cell* **126**, 663–676 (2006).
38. C. M. Metallo, L. Ji, J. J. de Pablo, S. P. Palecek, Retinoic acid and bone morphogenetic protein signaling synergize to efficiently direct epithelial differentiation of human embryonic stem cells. *Stem Cells* **26**, 372–380 (2008).
39. T. Kadoshima, H. Sakaguchi, T. Nakano, M. Soen, S. Ando, M. Eiraku, Y. Sasai, Self-organization of axial polarity, inside-out layer pattern, and species-specific progenitor dynamics in human ES cell–derived neocortex. *Proc. Natl. Acad. Sci. U.S.A.* **110**, 20284–20289 (2013).
40. A. Stathopoulos, M. Levine, Genomic regulatory networks and animal development. *Dev. Cell* **9**, 449–462 (2005).
41. L. Jiménez-Rojo, Z. Granchi, D. Graf, T. A. Mitsiadis, Stem cell fate determination during development and regeneration of ectodermal organs. *Front. Physiol.* **3**, 107 (2012).
42. M.-X. Lei, C.-M. Chuong, R. B. Widelitz, Tuning Wnt signals for more or fewer hairs. *J. Invest. Dermatol.* **133**, 7–9 (2013).
43. X. Lim, R. Nusse, Wnt signaling in skin development, homeostasis, and disease. *Cold Spring Harb. Perspect. Biol.* **5**, a008029 (2013).
44. C. Niemann, F. M. Watt, Designer skin: Lineage commitment in postnatal epidermis. *Trends Cell Biol.* **12**, 185–192 (2002).
45. E. E. Kandyba, M. B. Hodgins, P. E. Martin, A murine living skin equivalent amenable to live-cell imaging: Analysis of the roles of connexins in the epidermis. *J. Invest. Dermatol.* **128**, 1039–1049 (2008).
46. E. Bellas, M. Seiberg, J. Garlick, D. L. Kaplan, In vitro 3D full-thickness skin-equivalent tissue model using silk and collagen biomaterials. *Macromol. Biosci.* **12**, 1627–1636 (2012).
47. K. Asakawa, K.-e. Toyoshima, N. Ishibashi, H. Tobe, A. Iwadate, T. Kanayama, T. Hasegawa, K. Nakao, H. Toki, S. Noguchi, M. Ogawa, A. Sato, T. Tsuji, Hair organ regeneration via the bioengineered hair follicular unit transplantation. *Sci. Rep.* **2**, 424 (2012).

Acknowledgments: We are grateful to T. Irie for the invaluable comments. **Funding:** This work was partially supported by a Grant-in-Aid for KIBAN (A) from the Ministry of Education, Culture, Sports, Science, and Technology (grant 25242041) and by a collaboration grant (to T.T.) from Organ Technologies Inc. This work was partially funded by Organ Technologies Inc. **Author contributions:** T.T. designed the research plan; R.T., J.I., A. Sugawara, K.-e.T., K.I., M. Ogawa, K.S., K.A., A.K., M. Oshima, and R.M. performed the experiments; A. Sato, T.Y., A.T., H.E., and T.T. discussed the results; and T.T., K.-e.T., and M. Ogawa wrote the paper. **Competing interests:** This work was performed under an invention agreement between the Tokyo University of Science, RIKEN, and Organ Technologies Inc. T.T. is a director at Organ Technologies Inc. **Data and materials availability:** All data needed to evaluate the conclusions in the paper are present in the paper and/or the Supplementary Materials. Additional data related to this paper may be requested from the authors.

Submitted 6 July 2015
Accepted 29 February 2016
Published 1 April 2016
10.1126/sciadv.1500887

Citation: R. Takagi, J. Ishimaru, A. Sugawara, K.-e. Toyoshima, K. Ishida, M. Ogawa, K. Sakakibara, K. Asakawa, A. Kashiwakura, M. Oshima, R. Minamide, A. Sato, T. Yoshitake, A. Takeda, H. Egusa, T. Tsuji, Bioengineering a 3D integumentary organ system from iPS cells using an in vivo transplantation model. *Sci. Adv.* **2**, e1500887 (2016).